

Optimal Transport for Brain-Image Alignment: Unveiling Redundancy and Synergy in Neural Information Processing

Yang Xiao^{1*} Wang Lu^{2#} Jie Ji³ Ruimeng Ye¹
Gen Li³ Xiaolong Ma³ Bo Hui^{1‡}

¹University of Tulsa, ²Tsinghua University, ³Clemson University

Abstract

The design of artificial neural networks (ANNs) is inspired by the structure of the human brain, and in turn, ANNs offer a potential means to interpret and understand brain signals. Existing methods primarily align brain signals with stimulus signals using Mean Squared Error (MSE), which focuses only on local point-wise alignment and ignores global matching, leading to coarse interpretations and inaccuracies in brain signal decoding.

In this paper, we address these issues through optimal transport (OT) and theoretically demonstrate why OT provides a more effective alignment strategy than MSE. Specifically, we construct a transport plan between brain voxel embeddings and image embeddings, enabling more precise matching. By controlling the amount of transport, we mitigate the influence of redundant information. We apply our alignment model directly to the Brain Captioning task by feeding brain signals into a large language model (LLM) instead of images. Our approach achieves state-of-the-art performance across ten evaluation metrics, surpassing the previous best method by an average of 6.11% in single-subject training and 3.81% in cross-subject training. Additionally, we have uncovered several insightful conclusions that align with existing brain research. We unveil the redundancy and synergy of brain information processing through region masking and data dimensionality reduction visualization experiments. We believe our approach paves the way for a more precise understanding of brain signals in the future. The code is available soon.

1. Introduction

The structure of the human brain has inspired the development of neural networks [51], and in recent years, research on brain-computer interfaces has gained increasing atten-

*First Author

†Corresponding Author

‡Corresponding Author

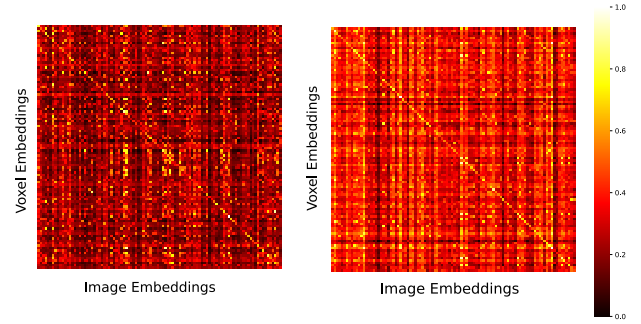


Figure 1. The left is MSE Heatmap and the right is OT Heatmap.

tion. Researchers have been exploring ways to leverage neural networks to decode brain signals and better understand brain function. Among various neural recording techniques, functional Magnetic Resonance Imaging (fMRI) provides an indirect measure of neural activity by capturing fluctuations in blood oxygen levels. With advances in deep learning, researchers have attempted to align fMRI signals with neural representations in pre-trained models to enhance brain decoding capabilities [41, 57].

As the main approach to interpreting brain region signals, brain-image alignment combines artificial intelligence and neuroscience, allowing us to decipher semantic information from neural activities in response to different types of stimuli [2, 20, 35, 52, 57, 69–71, 75, 77]. By projecting data in a shared embedding space, information from different modalities can be mapped to the same dimensional space, ensuring semantic consistency [26, 30, 49, 68]. By aligning fMRI with the image using deep learning methods, researchers implemented the aligned model for downstream tasks, such as Visual Description [71, 72], Image Generation [35, 57, 72], Object Detection [71], Image Retrieval [72]. These advances open up new possibilities for understanding human cognition and developing brain-computer interfaces.

Although brain-image alignment has made significant progress, previous research methods have not considered the differences between brain signal representations and

real-world physical signal representations. These methods mainly focus on point-to-point alignment, leading to misalignment and redundancy. Specifically, most alignment approaches rely on mean squared error (MSE) loss or contrastive InfoNCE loss [42]. However, these batch-level loss functions primarily focus on minimizing direct distance metrics, potentially overlooking complex non-linear relationships in cross-modal alignment. As shown in Fig. 1, MSE can only capture point-wise relationships resulting in highlighted correlations only along the diagonal, while failing to capture global relationships, leading to weak correlations in other areas. Consequently, the underlying mechanisms of alignment remain insufficiently explored [59].

To solve the above issues, we analyzed the mathematical principle of MSE alignment. Different modalities can naturally be interpreted as different probability distributions, and aligning these distributions can be formulated as an Optimal Transport (OT) problem [62]. We found that MSE is equivalent to a special case of OT, namely the problem of optimizing a quadratic cost function (Euclidean distance) when the transport plan is fixed to the identity matrix. However, MSE does not consider whether a better matching strategy exists. Instead, it directly computes the error based on point-wise matching, which can easily lead to local optima. In contrast, general optimal transport builds upon MSE by allowing more flexible matching between different points and considering the alignment of two distributions from a global perspective. Compared to MSE, this approach is more effective in achieving a globally optimal solution. Thus, we propose to use the OT method to achieve brain-image alignment.

We can obtain an optimized transport plan by optimizing the cost matrix, which depends on the distance between one distribution and another. Hence, the optimization of the OT problem is equivalent to learning the valid representations in machine learning [29]. We constructed a new loss function based on OT (See in Fig. 2). We proved that MSE loss is a special case of OT loss. As shown in the OT heatmap (See in Fig. 1), compared to MSE, the OT heatmap highlights points outside the diagonal, indicating that it also captures relationships beyond point-wise correspondences. Therefore, OT not only considers the point-wise alignment of MSE but also takes into account the impact of the overall distribution. By optimizing the loss function, we achieved the **SOTA** results on downstream tasks much better than MSE loss.

We also verify the existing research conclusions about the brain in cognitive neuroscience from the perspective of deep learning. The brain processes information in both **redundant** and **synergistic** ways [36]. Receiving both types of information means that the brain can **maintain robustness** by utilizing redundant information while achieving **better processing performance** through synergistic. Re-

dundancy means that increasing the amount of transport information does not always yield optimal outcomes, as excessive information flow may introduce noise or inefficiencies. Therefore, we explored the impact of restricting the mass of transport information on alignment evaluation (See in Fig. 5). At the same time, the Synergistic nature of brain function is closely tied to its modular organization [61]. Different brain areas (called Brodmann’s Areas) process different semantic information (See in Fig. 3) [8]. These areas are universally recognized and widely utilized as a standardized anatomical framework for mapping neuropsychological functions within the cerebral cortex [61]. Based on the brain activation, NSD dataset divides the effectively activated cortex into five major brain regions (A brain region consists of multiple brain areas.): 1) Vision: V1, V2, V3, and V4. 2) Body: EBA, FBA-1, FBA-2, and mTL-bodies (‘mid temporal lobe bodies’). 3) Face: OFA, FFA-1, FFA-2, and mTL-faces (‘mid temporal lobe faces’). 4) Place: OPA, PPA, and RSC. 5) Word: OWFA, VWFA-1, VWFA-2, mfs-words (‘mid fusiform sulcus words’), and mTL-words (‘mid temporal lobe words’). On this basis, we not only analyzed the redundancy (See in Tab. 2 and Fig. 6) and the synergy (See in Tab. 2 and Fig. 6) between different regions but also examined their differences and importance (See in Fig. 4).

The following are our contributions:

- **In theory**, We discussed the gap between MSE and OT from the perspective of mathematical derivation and correlation visualization heatmaps and proved that OT Loss can not only learn the point-wise relationship in MSE but also capture the relationship beyond point-wise.
- **In method**, We established an alignment model between fMRI and images through Optimal Transport methods. The aligned model was then used to test in the pre-trained large language model (LLM), achieving the SOTA in image description by decoding brain fMRI signals.
- **In analysis**, Our experimental results confirm the presence of both redundancy and synergy in neural information processing. By leveraging PCA and UMAP, we effectively visualized these characteristics, providing deeper insights.

2. Related Work

2.1. Brain-Image Alignment.

Brain-Image Alignment includes EEG-Image Alignment [5, 9] and fMRI-Image Alignment [47, 48, 57, 71, 73]. The goal is to map the neural modality into a common latent space for downstream tasks. Some methods attempt to predict brain responses by taking images as input [55, 73, 76]. The similarity between ANNs and Brain Neural Network (BNNs) is then quantified based on the correlation between the predicted and actual brain responses, a metric known

as the Brain Score [55]. Some methods attempt to use recorded brain responses as the condition to train diffusion models for image generation [5, 43, 56, 57, 63]. Brain Caption aims to generate textual descriptions of a given image based on brain responses rather than the image itself [17, 17, 22, 37, 58, 64, 71].

2.2. Optimal Transport.

Optimal Transport (OT) is a fundamental mathematical framework that seeks to find the most efficient way to transport information or mass from one probability distribution to another [13]. It has been widely studied in probability theory, optimization, and machine learning, with applications spanning image processing, generative modeling, and domain adaptation. The Monge Problem [39] aims to find the best mapping pattern to match two different distributions. Kantorovich formulation [28] provides the solution to take the Monge problem into a linear programming problem. A key metric derived from Kantorovich’s formulation is the Wasserstein distance, which quantifies the optimal transport cost between two probability distributions. The discrete version of the Wasserstein-1 distance was introduced to the image databases as a measure of the minimal effort required to transform one distribution into another by redistributing mass [53]. Many works have successfully applied OT to image classification [21, 59, 60], graph learning [7, 11, 45], transfer learning [12, 33, 34].

2.3. Brodmann’s Areas

Brodman’s Areas [8] is universally recognized and widely utilized as a standardized anatomical framework for mapping neuropsychological functions within the cerebral cortex [61]. These regions, originally defined based on cytoarchitectonic differences, are associated with distinct cognitive, sensory, and motor functions, which work on visual information processing [18], spatial navigation [16], facial recognition [54], words decoding [19] or action understanding [40]. After visual information enters the human brain, it goes to different partitions and gradually forms representations from primary to advanced levels [74]. The primary visual cortex (V1) is responsible for processing basic visual information [74], such as orientation and spatial frequency. The Face region includes many areas that are responsible for the initial analysis and integration of facial information, playing a role in emotional processing, and social cognitive activities, and are capable of handling more detailed visual processing [46, 50]. The Word region consists of numerous areas responsible for processing early visual features of text, recognizing words as whole units, and understanding their semantic meanings [14, 67]. The Place region plays a key role in processing visual geometric features, background information, and spatial memory [1, 15, 27]. The Body Area primarily processes body shape informa-

tion, motion perception, and the emotional expression of movements [4, 65].

3. Problem Setup

3.1. Preliminary

Let X and Y be metric spaces, f and g be fMRI encoder and image encoder. In this paper, X refers to brain signals and Y refers to images where x is a sample point in $f(X)$ and y is a sample point in $g(Y)$. Let μ and ν be probability distributions defined on these spaces:

$$x \sim \mu, x \in f(X); y \sim \nu, y \in g(Y) \quad (1)$$

Since $g(Y)$ is a fixed pre-trained weight, our parameter update only involves $f(X)$.

3.2. Mean Squared Error (MSE)

A common approach for aligning embeddings is using the Mean Squared Error (MSE) loss. Considering a batch of N fMRI-image pairs $\{(\mathbf{x}_i, \mathbf{y}_i)\}_i^N$ which is defined as:

$$L_{MSE}(\mathbf{x}, \mathbf{y}) = \frac{1}{N} \sum_{i=1}^N \|\mathbf{x}_i - \mathbf{y}_i\|^2 \quad (2)$$

where \mathbf{x}_i and \mathbf{y}_i represent the corresponding embeddings. While MSE is a simple and widely used loss function, it has several limitations when applied to aligning distributions:

- **Pointwise comparison:** MSE computes the Euclidean distance between corresponding points but does not consider the overall structure of the distributions.
- **Distribution mismatch:** If μ and ν have different support (e.g., discrete vs. continuous distributions), MSE may not provide meaningful alignment.
- **Sensitivity to outliers:** MSE is highly influenced by outliers, which can distort the optimization process.
- **Lack of geometric awareness:** MSE does not account for the underlying geometry of the data space, making it less effective in aligning complex distributions.

4. Method

4.1. Framework

In this section, we will explore how the optimal transport method is applied to our task and how its loss function not only encompasses but also surpasses the MSE loss. While preserving the point-wise training process of MSE, the optimal transport loss additionally captures global relationships, resulting in improved alignment and more powerful model performance.

As shown in Fig. 2, the brain signals are generated by inputting image stimulus. We use fMRI Encoder and a pretrained CLIP Image Encoder to encode both two types of data into the same embedding space. We compute the

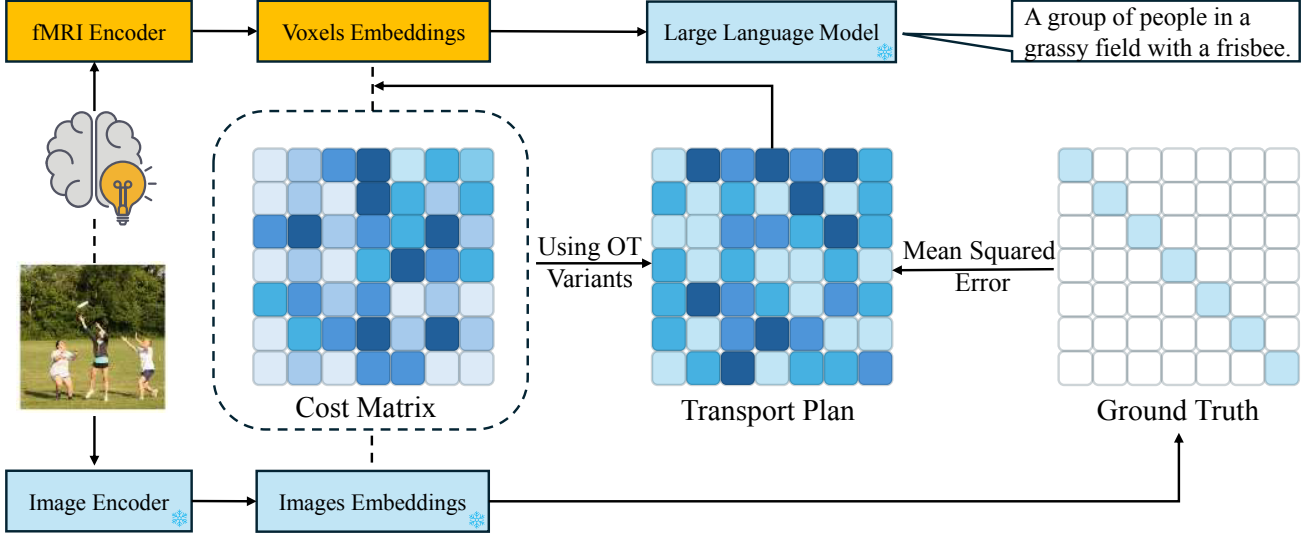


Figure 2. Framework: our OT Loss not only considers the point-wise alignment of MSE but also the global relationships.

wasserstein-2 distance of two embeddings as a cost matrix. From the point-wise perspective, we need to compute the MSE distance between pairs of embeddings. From the distribution alignment perspective, we need to measure the global relationships of one distribution on a single point of the other distribution. Ultimately, this forms our transport plan to optimize the loss function and update the model parameters.

4.2. Optimal Transport

The Monge Optimal Transport problem [39] aims to find to a best mapping $T : X \rightarrow Y$ to transport the source distribution μ to target distribution ν with the least cost C :

$$\min_T \int_X C(\mathbf{x}, T(\mathbf{x})) d\mu(\mathbf{x}) \quad (3)$$

Where T needs to satisfy the push-forward constraint:

$$T_{\#}\mu = \nu \quad (4)$$

For all measurable sample sets $S \subseteq Y$, we have

$$\mu(T^{-1}(S)) = \nu(S) \quad (5)$$

To find a solution of a given OT problem, the Kantorovich formulation [28] relaxes the mapping constraint in the Monge formulation, allowing the consideration of a joint distribution (transport plan) $\gamma(\mathbf{x}, \mathbf{y})$, thereby transforming the problem into a linear programming problem:

$$\min_{\gamma \in \Pi(\mu, \nu)} \int_{X \times Y} C(\mathbf{x}, \mathbf{y}) d\gamma(\mathbf{x}, \mathbf{y}) \quad (6)$$

Where $\Pi(\mu, \nu)$ denotes the set of all joint distributions satisfying the marginal constraints:

$$\int_Y \gamma(\mathbf{x}, \mathbf{y}) d\mathbf{y} = \mu(\mathbf{x}), \quad \int_X \gamma(\mathbf{x}, \mathbf{y}) d\mathbf{x} = \nu(\mathbf{y}) \quad (7)$$

The Wasserstein distance addresses both the feasibility issue of Monge and the interpretability issue of Kantorovich. The Wasserstein-p distance is given by:

$$W_p(\mu, \nu) = \left(\inf_{\gamma \in \Pi(\mu, \nu)} \int_{X \times Y} \|\mathbf{x} - \mathbf{y}\|^p d\gamma(\mathbf{x}, \mathbf{y}) \right)^{\frac{1}{p}} \quad (8)$$

Specifically, we use $p=2$ in our experiments.

Let \mathbf{x} be the brain voxel embedding and \mathbf{y} be the image embedding. The Wasserstein-2 distance directly measures the discrepancy between the probability distributions μ and ν , considering both local pointwise differences and global relationships.

4.3. OT Loss and MSE Loss

We define the cost matrix:

$$C_{i,j} = \|\mathbf{x}_i - \mathbf{y}_j\|^2 \quad (9)$$

where the diagonal of C represents the Euclidean distance between corresponding points, and the off-diagonal elements account for global relationships.

The size of this cost matrix C is $\mathbb{R}^{N \times M}$, where N is the number of brain voxel embeddings and M is the number of image embeddings. (Specially, $N = M$ in our dataset.) Then, to compute the optimal transport plan, we assume

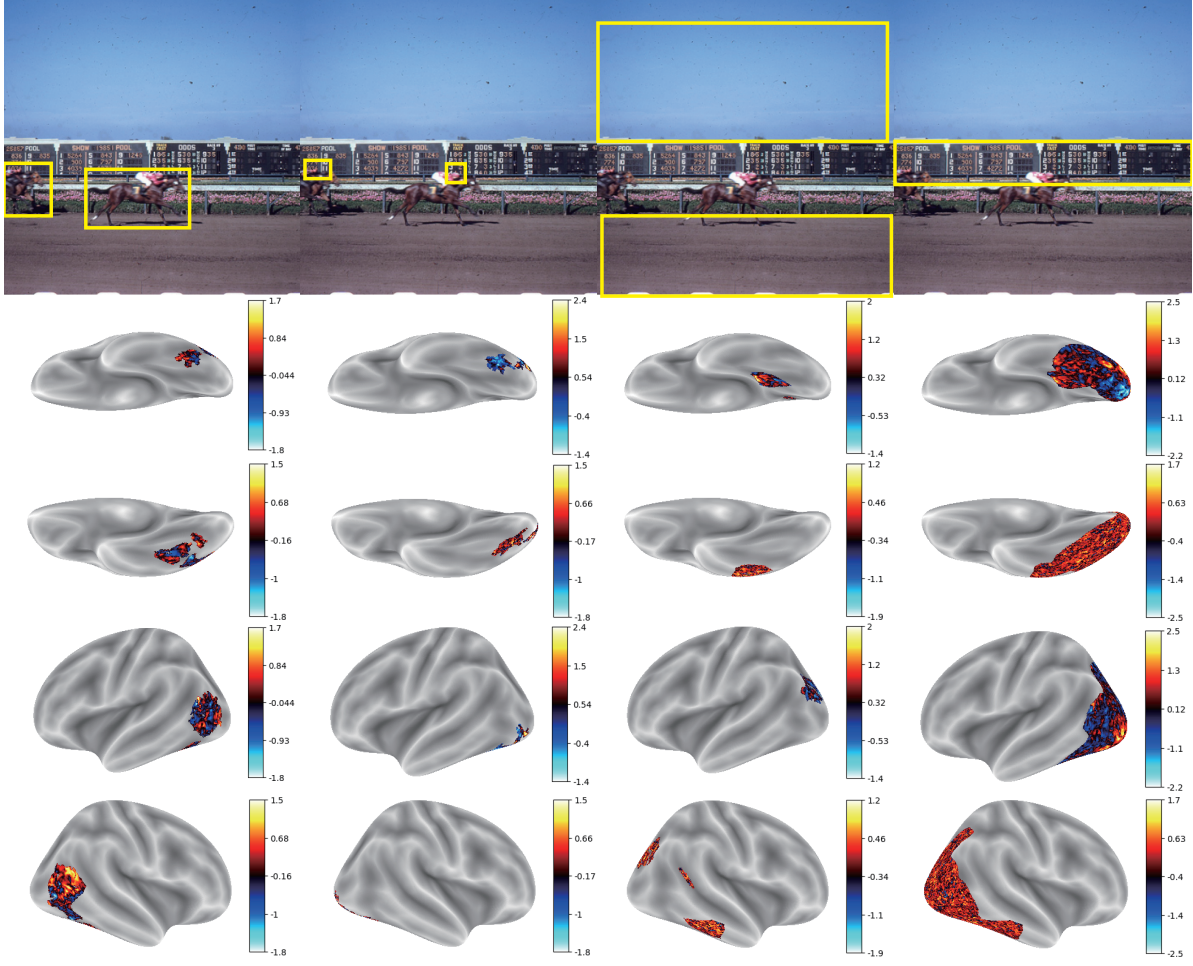


Figure 3. Each row of brain images from upper to down is related to left ventral, right ventral, left lateral, and right lateral. Each column from left to right is related to Body, Face, Place, and Word region.

uniform weight distributions:

$$\mu' = \left(\frac{1}{N}, \frac{1}{N}, \dots, \frac{1}{N} \right), \quad \nu' = \left(\frac{1}{N}, \frac{1}{N}, \dots, \frac{1}{N} \right) \quad (10)$$

We define λ as the mass ratio that controls m , the amount of transport:

$$m = \lambda \min \left(\sum_i \mu'_i, \sum_j \nu'_j \right). \quad (11)$$

The optimal transport plan is obtained by solving:

$$\gamma^* = \operatorname{argmin}_{\gamma} \sum_{i=1}^N \sum_{j=1}^N \gamma_{i,j} C_{i,j} \quad (12)$$

subject to:

$$\sum_i \gamma_{i,j} \leq \mu'_i, \quad \sum_j \gamma_{i,j} \leq \nu'_j, \quad \sum_{i,j} \gamma_{i,j} = m. \quad (13)$$

We define the Optimal Transport Loss (OT Loss) as:

$$L_{OT} = \sum_{i=1}^N \sum_{j=1}^N \gamma_{i,j}^* C_{i,j} \quad (14)$$

which minimizes the Wasserstein-2 transport cost.

By comparing this with the definition of Wasserstein-2 distance:

$$W_2^2(\mu, \nu) = L_{OT} = \sum_{i=1}^N \sum_{j=1}^N \gamma_{i,j}^* C_{i,j}. \quad (15)$$

To understand the connection between OT Loss and MSE, we rewrite:

$$\begin{aligned} L_{OT} &= \sum_{i=1}^N \gamma_{i,i}^* C_{i,i} + \sum_{i=1}^N \sum_{j \neq i}^N \gamma_{i,j}^* C_{i,j} \\ &= \sum_{i=1}^N \gamma_{i,i}^* \|\mathbf{x}_i - \mathbf{y}_i\|^2 + \sum_{i=1}^N \sum_{j \neq i}^N \gamma_{i,j}^* C_{i,j} \end{aligned} \quad (16)$$

If γ^* is an identity matrix (i.e., mass transport only occurs between corresponding pairs $(\mathbf{x}_i, \mathbf{y}_i)$), then:

$$L_{OT} = \sum_{i=1}^N 1 \times C_{i,i} + \sum_{i=1}^N \sum_{j \neq i}^N 0 \times C_{i,j} \quad (17)$$

$$L_{OT} \approx L_{MSE} \quad (18)$$

which means that MSE is a special case of OT Loss where only diagonal elements contribute. However, in general, OT Loss incorporates a more holistic measure of distribution alignment by considering global transport relationships.

For the model’s parameter θ , the parameters updating is:

$$\begin{aligned} \nabla_{\theta} L_{OT} &= \sum_{i=1}^N 2\gamma_{i,i}^* \nabla_{\theta} f(X_i)(\mathbf{x}_i - \mathbf{y}_i) \\ &+ \sum_{i=1}^N \sum_{j \neq i}^N 2\gamma_{i,j}^* \nabla_{\theta} f(X_i) \frac{\partial C_{i,j}}{\partial \mathbf{x}_i} \end{aligned} \quad (19)$$

$$\theta \leftarrow \theta - \eta \nabla_{\theta} L_{OT} \quad (20)$$

Where η is the learning rate.

5. Experiment

5.1. Experiment Setup

We ran all experiments and visualization in Natural Scenes Dataset (NSD) [2] which contains images from COCO [32] and corresponding fMRI signals recorded in their experiments. Due to spatial distortion and/or head displacement over the course of a scan session, voxels on the edges of the imaged volume may not obtain a full set of data for that session. In pre-processing, such voxels are detected, deemed “invalid”, and are essentially set to 0 for the whole scan session. For the most part, brain voxels of interest are almost always valid. We use the valid voxels as our fMRI part. The dataset spans 8 subjects who were scanned for 30-40 hours (30-40 separate scanning sessions), where each session consisted of viewing 750 images for 3 seconds each. Images were seen 3 times each across the sessions and were unique to each subject, except for a select 1,000 images which were seen by all the subjects. Four subjects (No. 1, 2, 5, and 7) who had completed all the sessions were selected. We choose the test set of subject 1 for evaluation. The model training follows two scenarios: single-subject training (subject 1) and cross-subject training (subjects 1, 2, 5, and 7). In cross-subject training, two subjects are randomly selected in each iteration to compute the OT Loss for parameter updates.

5.2. Alignment Experiments

Image Encoder. We use the CLIP (Vision Transformer, Large, Patch Size 14, ViT-L/14) model trained by OpenAI

to encode image input. This model was trained on a 400M image-text pair dataset constructed by OpenAI, which is larger and more diverse than ImageNet. The extensive training data enables CLIP to generalize across multiple tasks without requiring task-specific fine-tuning. We leverage the pre-trained weights to encode images and align them with corresponding fMRI signals through self-supervised learning, projecting them into an embedding space. Since the pre-trained weights remain frozen, the image embeddings do not change during training, ensuring a stable representation of visual input. This stability facilitates a controlled alignment process between the vision and neural modalities.

fMRI Encoder. We trained a transformer-based encoder [25, 71] to map brain voxel signals into the same embedding space as image embeddings for alignment. Transformers are particularly effective in capturing long-range dependencies across voxel signals, making them well-suited for modeling complex neural representations. The fMRI Encoder computes self-attention and cross-attention over voxel-level fMRI signals to capture both intra-modal and cross-modal dependencies. It employs cross-attention mechanisms to condense high-dimensional voxel representations into a latent bottleneck, facilitating dimensionality reduction while preserving essential information. In this process, the key (K) and value (V) are derived from projections of the input tokens, while the query (Q) originates from learnable latent queries. By learning a shared representation, the model aligns fMRI signals with image embeddings, enabling effective cross-modal correspondence.

Alignment and Brain Captioning. We aligned the voxel embeddings to image embeddings via OT loss. In evaluation, we use shikra [10] as the LLM for the brain caption task (Image Description via feeding fMRI instead of image). The LLM will load the voxel embedding instead of image embedding to describe the details of the image. There are a total of 982 samples per subject. Ground truth captions are retrieved from COCO [32], and evaluation of inferred captions uses five standard metrics: BLEU-k [44], METEOR [6], ROUGE-L [31], CIDEr [66], and SPICE [3], CLIP-S [49], and RefCLIP-S [23]. During evaluation, we will freeze the weights of the pre-trained LLM. As shown in Tab. 1, the first gray row is the result of directly feeding the image into the LLM for evaluation, and this is the gold standard we should try to approach and exceed. Compared with existing methods [17, 22, 37, 58, 63, 71], our method achieves SOTA for all metrics in this table. Compared with the best UMBRAE-S1 and the best UMBRAE (Cross Subjects), our method increases average 6.11% and 3.81%.

5.3. Redundant and Synergistic Interactions

To validate the redundant interactions in brain information processing, we adjusted the mass ratio in the optimal transport process using the hyper-parameter λ . As shown in

Method	BLEU1	BLEU2	BLEU3	BLEU4	METEOR	ROUGE	CIDEr	SPICE	CLIP-S	RefCLIP-S
Shikra-w/img	82.38	69.9	58.63	49.66	35.6	65.49	161.43	27.62	80.6	85.92
SDRecon [63]	36.21	17.11	7.72	3.43	10.03	25.13	13.83	5.02	61.07	66.36
OneLLM [22]	47.04	26.97	15.49	9.51	13.55	35.05	22.99	6.26	54.8	61.28
UniBrain [37]	None	None	None	None	16.90	22.20	None	None	None	None
BrainCap [17]	55.96	36.21	22.7	14.51	16.68	40.69	41.3	9.06	64.31	69.9
[58]	57.19	37.17	23.78	15.85	18.6	36.67	49.51	12.39	65.49	None
UMBRAE-S1 [71]	57.63	38.02	25.00	16.76	18.41	42.15	51.93	11.83	66.44	72.12
UMBRAE [71]	59.44	40.48	27.66	19.03	19.45	43.71	61.06	12.79	67.78	73.54
UMBRAE(MSE)-S1*	57.33	37.69	24.88	16.83	18.23	41.61	51.50	11.86	66.47	72.21
UMBRAE(MSE)*	59.02	39.9	27.1	18.94	19.08	43.41	58.8	12.68	67.87	73.55
OT-S1	63.25	44.76	30.96	21.72	21.61	47.12	71.52	14.41	70.35	75.68
OT-Cross Subjects	64.12	45.18	31.16	21.50	21.42	46.83	72.90	14.51	69.95	75.44

Table 1. Results: all the results cited or we provided are evaluated in the pre-trained shikra.

V	P	F	W	B	Other	BLEU1	BLEU2	BLEU3	BLEU4	METEOR	ROUGE	CIDEr	SPICE	CLIP-S	RefCLIP-S	Valid Voxels
●	●	●	●	●	●	63.25	44.76	30.96	21.72	21.61	47.12	71.52	14.41	70.35	75.68	15724/15724
●	○	○	○	○	○	43.11	21.68	10.23	5.48	10.65	31.64	10.95	3.03	46.24	52.94	4657/15724
○	●	○	○	○	○	48.14	27.75	15.09	8.72	13.25	35.23	23.00	6.03	54.25	60.32	2252/15724
○	○	●	○	○	○	44.87	23.02	10.89	5.42	11.47	32.58	12.33	3.94	49.10	55.65	1042/15724
○	○	○	●	○	○	42.68	20.44	9.16	4.61	10.19	31.45	8.31	2.22	43.99	50.71	1736/15724
○	○	○	○	●	○	53.09	32.85	20.38	12.99	15.78	39.05	37.18	8.56	58.23	64.70	2934/15724
○	●	●	●	○	○	59.28	39.66	25.91	16.9	18.92	43.52	55.59	11.74	66.13	71.86	6706/15724
●	●	●	●	○	○	61.56	42.43	28.65	19.58	19.98	45.05	62.83	12.83	67.34	73.03	11051/15724

Table 2. Region of Interest.

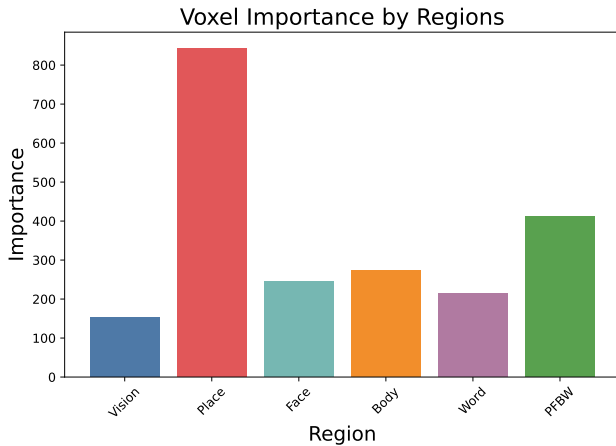


Figure 4. The regions’ importance.

Fig. 5, when the ratio exceeds a certain constant such as 0.3, the model exhibits robust performance. We arbitrarily selected one metric (CIDEr), but in fact, all metrics follow this trend. More detailed results can be seen in table in the appendix A.1.

We explored synergistic interactions from the perspective of Brodmann’s areas, specifically analyzing the coordination among brain regions related to Vision, Place, Body,

Face, and Word. Previous studies have shown that the visual cortex primarily processes low-level information, while certain cortical areas are involved in processing high-level representations. As observed from our experimental results (see Table 2), the performance of a single region approach is suboptimal, and different regions’ effects are significant differences while multiple regions working in synergy significantly improve performance.

As shown in Fig. 3 and 7, different regions carry different semantic information. Depending on the information contained in the images, the activation situation is also different, for instance, all images contain place information, but not necessarily word information. These semantic attributes influence the activation of different brain regions. To further investigate the contribution of each area to the alignment task, we employed gradient perturbation analysis and voxel-based weighting for evaluation. The results indicate that the visual region has the lowest importance, whereas the Place region exhibits the highest importance(See in Fig. 4). This not only corroborates the previous conclusion that the visual cortex primarily processes low-level information but also confirms the ubiquity of Place-related information in images.

We employed PCA [24] and UMAP [38] to visualize embeddings under both single region and multi regions, aiming

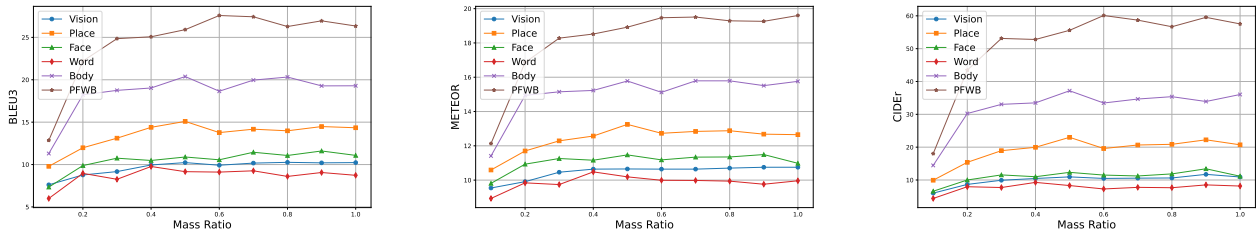


Figure 5. The Redundant and Synergistic of three metrics in different regions

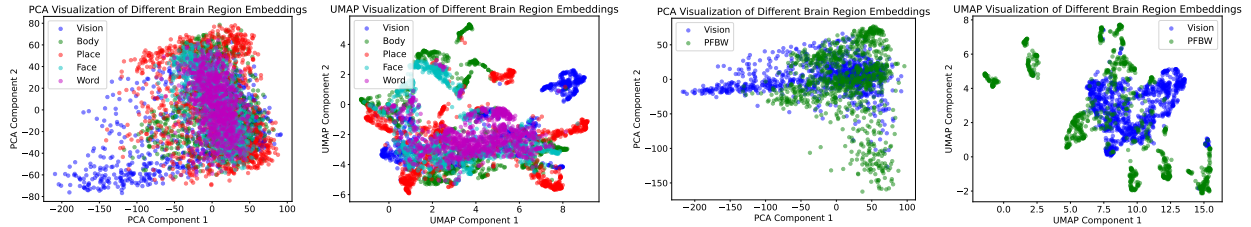


Figure 6. Visualization

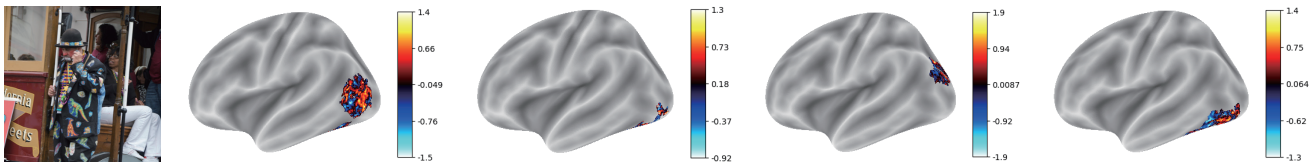


Figure 7. Case study: Ground Truth, Body Region, Face Region, Place Region, Word Region.

to explore their differences. The results indicate that in the visualization of the single region, embeddings appear noticeably entangled and interwoven, which may be attributed to redundant interactions. In contrast, under multi-region synergy, the visualization reveals a clear separation between synergistic embeddings and vision embeddings, potentially reflecting the influence of synergistic interactions (See in Fig. 6).

In summary, redundancy maintains the robustness of information processing in the brain when external stimuli change, while synergy enables multiple brain regions to collaborate for more efficient information processing. our work made the redundancy and synergy of brain information processing more explicit.

5.4. Ablation Studies

Keeping the experimental hyper-parameters and the network architecture unchanged, we replaced the loss function with MSE loss. The results demonstrate that in single-subject training (See in Tab. 1, UMBRAE(MSE)-S1*), all evaluation metrics showed improvement, with an average increase of 6.28% per evaluation metric. In cross-subject training (See in Tab. 1, UMBRAE(MSE)*), all metrics also exhibited enhancements, with an average improvement of

4.27% per evaluation metric. Then, we calculate the embeddings of the same data set based on two models for correlation analysis. As shown in Fig. 1, MSE primarily captures point-wise relationships, resulting in strong correlations only along the diagonal, while failing to account for global relationships. OT extends beyond point-wise correspondences by highlighting correlations beyond the diagonal, demonstrating its ability to capture global structural relationships. Thus, OT not only preserves the point-wise alignment inherent in MSE but also considers the overall distribution, leading to a more comprehensive representation.

6. Conclusion

In this paper, we propose an OT-based framework for brain-image alignment, capturing both local and global relationships for better alignment. We first proved why OT exceed MSE. Next, our experiments achieved SOTA in the brain caption task. Finally, we reveal the role of redundancy in neural robustness and synergy of brain regions through Brodmann’s area analysis. This work bridges neuroscience and deep learning, offering new insights.

References

- [1] Andrew S Alexander, Ryan Place, Michael J Starrett, Elizabeth R Christil, and Douglas A Nitz. Rethinking retrosplenial cortex: perspectives and predictions. *Neuron*, 111(2): 150–175, 2023. 3
- [2] Emily J Allen, Ghislain St-Yves, Yihan Wu, Jesse L Breedlove, Jacob S Prince, Logan T Dowdle, Matthias Nau, Brad Caron, Franco Pestilli, Ian Charest, et al. A massive 7t fmri dataset to bridge cognitive neuroscience and artificial intelligence. *Nature neuroscience*, 25(1):116–126, 2022. 1, 6
- [3] Peter Anderson, Basura Fernando, Mark Johnson, and Stephen Gould. Spice: Semantic propositional image caption evaluation. In *Computer Vision—ECCV 2016: 14th European Conference, Amsterdam, The Netherlands, October 11–14, 2016, Proceedings, Part V 14*, pages 382–398. Springer, 2016. 6
- [4] Serguei V Astafiev, Christine M Stanley, Gordon L Shulman, and Maurizio Corbetta. Extrastriate body area in human occipital cortex responds to the performance of motor actions. *Nature neuroscience*, 7(5):542–548, 2004. 3
- [5] Yunpeng Bai, Xintao Wang, Yan-Pei Cao, Yixiao Ge, Chun Yuan, and Ying Shan. Dreamdiffusion: High-quality eeg-to-image generation with temporal masked signal modeling and clip alignment. In *European Conference on Computer Vision*, pages 472–488. Springer, 2024. 2, 3
- [6] Satanjeev Banerjee and Alon Lavie. Meteor: An automatic metric for mt evaluation with improved correlation with human judgments. In *Proceedings of the acl workshop on intrinsic and extrinsic evaluation measures for machine translation and/or summarization*, pages 65–72, 2005. 6
- [7] Gary Bécigneul, Octavian-Eugen Ganea, Benson Chen, Regina Barzilay, and Tommi S Jaakkola. Optimal transport graph neural networks. 2020. 3
- [8] Korbinian Brodmann. *Vergleichende Lokalisationslehre der Grosshirnrinde in ihren Prinzipien dargestellt auf Grund des Zellenbaues*. Barth, 1909. 2, 3
- [9] Chi-Sheng Chen and Chun-Shu Wei. Mind’s eye: Image recognition by eeg via multimodal similarity-keeping contrastive learning. *arXiv preprint arXiv:2406.16910*, 2024. 2
- [10] Keqin Chen, Zhao Zhang, Weili Zeng, Richong Zhang, Feng Zhu, and Rui Zhao. Shikra: Unleashing multimodal llm’s referential dialogue magic. *arXiv preprint arXiv:2306.15195*, 2023. 6
- [11] Qihao Cheng, Da Yan, Tianhao Wu, Zhongyi Huang, and Qin Zhang. Computing approximate graph edit distance via optimal transport. *Proceedings of the ACM on Management of Data*, 3(1):1–26, 2025. 3
- [12] Nicolas Courty, Rémi Flamary, Devis Tuia, and Alain Rakotomamonjy. Optimal transport for domain adaptation. *IEEE transactions on pattern analysis and machine intelligence*, 39(9):1853–1865, 2016. 3
- [13] Marco Cuturi. Sinkhorn distances: Lightspeed computation of optimal transport. *Advances in neural information processing systems*, 26, 2013. 3
- [14] Stanislas Dehaene and Laurent Cohen. The unique role of the visual word form area in reading. *Trends in cognitive sciences*, 15(6):254–262, 2011. 3
- [15] Russell Epstein, Alison Harris, Damian Stanley, and Nancy Kanwisher. The parahippocampal place area: recognition, navigation, or encoding? *Neuron*, 23(1):115–125, 1999. 3
- [16] Norsiah Fauzan and Normardina Abdul Rahim. Brain waves in response to al-quran & dhikr. *Implementing Quranic values in society*, pages 145–157, 2015. 3
- [17] Matteo Ferrante, Furkan Ozelcik, Tommaso Boccatto, Rufin VanRullen, and Nicola Toschi. Brain captioning: Decoding human brain activity into images and text. *arXiv preprint arXiv:2305.11560*, 2023. 3, 6, 7
- [18] Mehmet Fişek, Dustin Herrmann, Alexander Egea-Weiss, Matilda Cloves, Lisa Bauer, Tai-Ying Lee, Lloyd E Russell, and Michael Häusser. Cortico-cortical feedback engages active dendrites in visual cortex. *Nature*, 617(7962):769–776, 2023. 3
- [19] Angela D Friederici. *Language in our brain: The origins of a uniquely human capacity*. MIT Press, 2017. 3
- [20] Zixuan Gong, Qi Zhang, Guangyin Bao, Lei Zhu, Ke Liu, Liang Hu, and Duoqian Miao. Mindtuner: Cross-subject visual decoding with visual fingerprint and semantic correction. *arXiv preprint arXiv:2404.12630*, 2024. 1
- [21] Dandan Guo, Zhuo Li, He Zhao, Mingyuan Zhou, Hongyuan Zha, et al. Learning to re-weight examples with optimal transport for imbalanced classification. *Advances in Neural Information Processing Systems*, 35:25517–25530, 2022. 3
- [22] Jiaming Han, Kaixiong Gong, Yiyuan Zhang, Jiaqi Wang, Kaipeng Zhang, Dahua Lin, Yu Qiao, Peng Gao, and Xiangyu Yue. Onellm: One framework to align all modalities with language. In *Proceedings of the IEEE/CVF Conference on Computer Vision and Pattern Recognition*, pages 26584–26595, 2024. 3, 6, 7
- [23] Jack Hessel, Ari Holtzman, Maxwell Forbes, Ronan Le Bras, and Yejin Choi. Clipscore: A reference-free evaluation metric for image captioning. *arXiv preprint arXiv:2104.08718*, 2021. 6
- [24] Harold Hotelling. Simplified calculation of principal components. *Psychometrika*, 1(1):27–35, 1936. 7
- [25] Andrew Jaegle, Felix Gimeno, Andy Brock, Oriol Vinyals, Andrew Zisserman, and Joao Carreira. Perceiver: General perception with iterative attention. In *International conference on machine learning*, pages 4651–4664. PMLR, 2021. 6
- [26] Chao Jia, Yinfei Yang, Ye Xia, Yi-Ting Chen, Zarana Parekh, Hieu Pham, Quoc Le, Yun-Hsuan Sung, Zhen Li, and Tom Duerig. Scaling up visual and vision-language representation learning with noisy text supervision. In *International conference on machine learning*, pages 4904–4916. PMLR, 2021. 1
- [27] Frederik S Kamps, Joshua B Julian, Jonas Kubilius, Nancy Kanwisher, and Daniel D Dilks. The occipital place area represents the local elements of scenes. *Neuroimage*, 132: 417–424, 2016. 3
- [28] L Kantorovich. On the transfer of masses (in russian). In *Doklady Akademii Nauk*, page 227, 1942. 3, 4

- [29] John Lee, Max Dabagia, Eva Dyer, and Christopher Rozell. Hierarchical optimal transport for multimodal distribution alignment. *Advances in neural information processing systems*, 32, 2019. 2
- [30] Gen Li, Nan Duan, Yuejian Fang, Ming Gong, and Daxin Jiang. Unicoder-vl: A universal encoder for vision and language by cross-modal pre-training. In *Proceedings of the AAAI conference on artificial intelligence*, pages 11336–11344, 2020. 1
- [31] Chin-Yew Lin. Rouge: A package for automatic evaluation of summaries. In *Text summarization branches out*, pages 74–81, 2004. 6
- [32] Tsung-Yi Lin, Michael Maire, Serge Belongie, James Hays, Pietro Perona, Deva Ramanan, Piotr Dollár, and C Lawrence Zitnick. Microsoft coco: Common objects in context. In *Computer Vision–ECCV 2014: 13th European Conference, Zurich, Switzerland, September 6–12, 2014, Proceedings, Part V 13*, pages 740–755. Springer, 2014. 6
- [33] Wang Lu, Yiqiang Chen, Jindong Wang, and Xin Qin. Cross-domain activity recognition via substructural optimal transport. *Neurocomputing*, 454:65–75, 2021. 3
- [34] Ying Lu, Liming Chen, and Alexandre Saidi. Optimal transport for deep joint transfer learning. *arXiv preprint arXiv:1709.02995*, 2017. 3
- [35] Andrew Luo, Maggie Henderson, Leila Wehbe, and Michael Tarr. Brain diffusion for visual exploration: Cortical discovery using large scale generative models. *Advances in Neural Information Processing Systems*, 36, 2024. 1
- [36] Andrea I Luppi, Pedro AM Mediano, Fernando E Rosas, Neegin Holland, Tim D Fryer, John T O’Brien, James B Rowe, David K Menon, Daniel Bor, and Emmanuel A Stamatakis. A synergistic core for human brain evolution and cognition. *Nature Neuroscience*, 25(6):771–782, 2022. 2
- [37] Weijian Mai and Zhijun Zhang. Unibrain: Unify image reconstruction and captioning all in one diffusion model from human brain activity. *arXiv preprint arXiv:2308.07428*, 2023. 3, 6, 7
- [38] Leland McInnes, John Healy, and James Melville. Umap: Uniform manifold approximation and projection for dimension reduction. *arXiv preprint arXiv:1802.03426*, 2018. 7
- [39] Gaspard Monge. Mémoire sur la théorie des déblais et des remblais. *Mem. Math. Phys. Acad. Royale Sci.*, pages 666–704, 1781. 3, 4
- [40] Aaron J Newman, Ted Supalla, Peter Hauser, Elissa L Newport, and Daphne Bavelier. Dissociating neural subsystems for grammar by contrasting word order and inflection. *Proceedings of the National Academy of Sciences*, 107(16):7539–7544, 2010. 3
- [41] Abdulhalik Oğuz and Ömer Faruk Ertuğrul. Introduction to deep learning and diagnosis in medicine. In *Diagnostic Biomedical Signal and Image Processing Applications with Deep Learning Methods*, pages 1–40. Elsevier, 2023. 1
- [42] Aaron van den Oord, Yazhe Li, and Oriol Vinyals. Representation learning with contrastive predictive coding. *arXiv preprint arXiv:1807.03748*, 2018. 2
- [43] Furkan Ozelik and Rufin VanRullen. Natural scene reconstruction from fmri signals using generative latent diffusion. *Scientific Reports*, 13(1):15666, 2023. 3
- [44] Kishore Papineni, Salim Roukos, Todd Ward, and Wei-Jing Zhu. Bleu: a method for automatic evaluation of machine translation. In *Proceedings of the 40th annual meeting of the Association for Computational Linguistics*, pages 311–318, 2002. 6
- [45] Hermina Petric Maretic, Mireille El Gheche, Giovanni Chierchia, and Pascal Frossard. Got: an optimal transport framework for graph comparison. *Advances in Neural Information Processing Systems*, 32, 2019. 3
- [46] David Pitcher, Vincent Walsh, and Bradley Duchaine. The role of the occipital face area in the cortical face perception network. *Experimental brain research*, 209:481–493, 2011. 3
- [47] Yansheng Qiu, Delin Chen, Hongdou Yao, Yongchao Xu, and Zheng Wang. Scratch each other’s back: Incomplete multi-modal brain tumor segmentation via category aware group self-support learning. In *Proceedings of the IEEE/CVF International Conference on Computer Vision*, pages 21317–21326, 2023. 2
- [48] Ruijie Quan, Wenguan Wang, Zhibo Tian, Fan Ma, and Yi Yang. Psychometry: An omnifit model for image reconstruction from human brain activity. In *Proceedings of the IEEE/CVF Conference on Computer Vision and Pattern Recognition*, pages 233–243, 2024. 2
- [49] Alec Radford, Jong Wook Kim, Chris Hallacy, Aditya Ramesh, Gabriel Goh, Sandhini Agarwal, Girish Sastry, Amanda Askell, Pamela Mishkin, Jack Clark, et al. Learning transferable visual models from natural language supervision. In *International conference on machine learning*, pages 8748–8763. PMLR, 2021. 1, 6
- [50] Gillian Rhodes, Patricia T Michie, Matthew E Hughes, and Graham Byatt. The fusiform face area and occipital face area show sensitivity to spatial relations in faces. *European Journal of Neuroscience*, 30(4):721–733, 2009. 3
- [51] Frank Rosenblatt. Principles of neurodynamics. perceptrons and the theory of brain mechanisms. Technical report, Cornell Aeronautical Lab Inc Buffalo NY, 1961. 1
- [52] Zvi N Roth, Kendrick Kay, and Elisha P Merriam. Natural scene sampling reveals reliable coarse-scale orientation tuning in human v1. *Nature communications*, 13(1):6469, 2022. 1
- [53] Yossi Rubner, Carlo Tomasi, and Leonidas J Guibas. A metric for distributions with applications to image databases. In *Sixth international conference on computer vision (IEEE Cat. No. 98CH36271)*, pages 59–66. IEEE, 1998. 3
- [54] Bart Rypma, Håkan Fischer, Anna Rieckmann, Nicholas A Hubbard, Lars Nyberg, and Lars Bäckman. Dopamine d1 binding potential predicts fusiform bold activity during face-recognition performance. *Journal of Neuroscience*, 35(44):14702–14707, 2015. 3
- [55] Martin Schrimpf, Jonas Kubilius, Ha Hong, Najib J Majaj, Rishi Rajalingham, Elias B Issa, Kohitij Kar, Pouya Bashivan, Jonathan Prescott-Roy, Franziska Geiger, et al. Brain-score: Which artificial neural network for object recognition is most brain-like? *BioRxiv*, page 407007, 2018. 2, 3
- [56] Paul Scotti, Atmadeep Banerjee, Jimmie Goode, Stepan Shabalin, Alex Nguyen, Aidan Dempster, Nathalie Verlinde,

- Elad Yundler, David Weisberg, Kenneth Norman, et al. Reconstructing the mind’s eye: fmri-to-image with contrastive learning and diffusion priors. *Advances in Neural Information Processing Systems*, 36, 2024. 3
- [57] Paul S Scotti, Mihir Tripathy, Cesar Kadir Torrico Villanueva, Reese Kneeland, Tong Chen, Ashutosh Narang, Charan Santhirasegaran, Jonathan Xu, Thomas Naselaris, Kenneth A Norman, et al. Mindeye2: Shared-subject models enable fmri-to-image with 1 hour of data. *arXiv preprint arXiv:2403.11207*, 2024. 1, 2, 3
- [58] Guobin Shen, Dongcheng Zhao, Xiang He, Linghao Feng, Yiting Dong, Jihang Wang, Qian Zhang, and Yi Zeng. Neuro-vision to language: Enhancing brain recording-based visual reconstruction and language interaction. In *The Thirty-eighth Annual Conference on Neural Information Processing Systems*. 3, 6, 7
- [59] Liangliang Shi, Jack Fan, and Junchi Yan. Ot-clip: Understanding and generalizing clip via optimal transport. In *Forty-first International Conference on Machine Learning*. 2, 3
- [60] Liangliang Shi, Haoyu Zhen, Gu Zhang, and Junchi Yan. Relative entropic optimal transport: a (prior-aware) matching perspective to (unbalanced) classification. *Advances in Neural Information Processing Systems*, 36, 2024. 3
- [61] Michael Strotzer. One century of brain mapping using brodmann areas. *Clinical Neuroradiology*, 19(3):179, 2009. 2, 3
- [62] Andrew M Stuart and Marie-Therese Wolfram. Inverse optimal transport. *SIAM Journal on Applied Mathematics*, 80(1):599–619, 2020. 2
- [63] Yu Takagi and Shinji Nishimoto. High-resolution image reconstruction with latent diffusion models from human brain activity. In *Proceedings of the IEEE/CVF Conference on Computer Vision and Pattern Recognition*, pages 14453–14463, 2023. 3, 6, 7
- [64] Yu Takagi and Shinji Nishimoto. Improving visual image reconstruction from human brain activity using latent diffusion models via multiple decoded inputs. *arXiv preprint arXiv:2306.11536*, 2023. 3
- [65] John C Taylor, Alison J Wiggett, and Paul E Downing. Functional mri analysis of body and body part representations in the extrastriate and fusiform body areas. *Journal of neurophysiology*, 98(3):1626–1633, 2007. 3
- [66] Ramakrishna Vedantam, C Lawrence Zitnick, and Devi Parikh. Cider: Consensus-based image description evaluation. In *Proceedings of the IEEE conference on computer vision and pattern recognition*, pages 4566–4575, 2015. 6
- [67] Mathieu Vigneau, Gaël Jobard, Bernard Mazoyer, and Nathalie Tzourio-Mazoyer. Word and non-word reading: what role for the visual word form area? *Neuroimage*, 27(3):694–705, 2005. 3
- [68] Shuai Wang, Daoan Zhang, Zipei Yan, Jianguo Zhang, and Rui Li. Feature alignment and uniformity for test time adaptation. In *Proceedings of the IEEE/CVF Conference on Computer Vision and Pattern Recognition*, pages 20050–20060, 2023. 1
- [69] Shizun Wang, Songhua Liu, Zhenxiong Tan, and Xinchao Wang. Mindbridge: A cross-subject brain decoding framework. In *Proceedings of the IEEE/CVF Conference on Computer Vision and Pattern Recognition*, pages 11333–11342, 2024. 1
- [70] Weihao Xia, Raoul de Charette, Cengiz Oztireli, and Jing-Hao Xue. Dream: Visual decoding from reversing human visual system. In *Proceedings of the IEEE/CVF Winter Conference on Applications of Computer Vision*, pages 8226–8235, 2024.
- [71] Weihao Xia, Raoul de Charette, Cengiz Oztireli, and Jing-Hao Xue. Umbræ: Unified multimodal brain decoding. In *European Conference on Computer Vision*, pages 242–259. Springer, 2024. 1, 2, 3, 6, 7
- [72] Fengyu Yang, Chao Feng, Daniel Wang, Tianye Wang, Ziyao Zeng, Zhiyang Xu, Hyoungseob Park, Pengliang Ji, Hanbin Zhao, Yuanning Li, et al. Neurobind: Towards unified multimodal representations for neural signals. *arXiv preprint arXiv:2407.14020*, 2024. 1
- [73] Huzheng Yang, James Gee, and Jianbo Shi. Brain decodes deep nets. In *Proceedings of the IEEE/CVF Conference on Computer Vision and Pattern Recognition*, pages 23030–23040, 2024. 2
- [74] Xiaoyan YE, Delong ZHANG, Song CHANG, and Ming LIU. The individual difference of visual mental imagery and its neural basis. *Advances in Psychological Science*, 26(7): 1186, 2018. 3
- [75] Qiongyi Zhou, Changde Du, Shengpei Wang, and Huiguang He. Clip-mused: Clip-guided multi-subject visual neural information semantic decoding. *arXiv preprint arXiv:2402.08994*, 2024. 1
- [76] Chengxu Zhuang, Siming Yan, Aran Nayebi, Martin Schrimpf, Michael C Frank, James J DiCarlo, and Daniel LK Yamins. Unsupervised neural network models of the ventral visual stream. *Proceedings of the National Academy of Sciences*, 118(3):e2014196118, 2021. 2
- [77] Futing Zou, Guo Wanxia, Emily J Allen, Yihan Wu, Ian Charest, Thomas Naselaris, Kendrick Kay, Brice A Kuhl, J Benjamin Hutchinson, and Sarah DuBrow. Re-expression of cal and entorhinal activity patterns preserves temporal context memory at long timescales. *Nature communications*, 14(1):4350, 2023. 1